

Geometry and physics in the deformations of crystalline caps

Jingyuan Chen and Zhenwei Yao*

*School of Physics and Astronomy, and Institute of Natural Sciences,
Shanghai Jiao Tong University, Shanghai 200240, China*

Elucidating the interplay of stress and geometry is a fundamental scientific question arising in multiple fields. In this work, we investigate the geometric frustration of crystalline caps confined on the sphere in both elastic and plastic regimes. Based on the revealed quasi-conformal ordering, we discover the partial, but uniform screening of the substrate curvature by the induced curvature underlying the inhomogeneous lattice. This scenario is fundamentally different from the conventional screening mechanism based on topological defects. In the plastic regime, the yield of highly stressed caps leads to fractures with featured morphologies not found in planar systems. We also demonstrate the strategy of engineering stress and fractures by vacancies. These results advance our general understanding on the organization and adaptivity of geometrically-frustrated crystalline order.

I. INTRODUCTION

Condensed matters confined on curved geometries are widely seen in multiple fields, [1, 2] ranging from protein shells [3–5] to liquid interfaces coated by colloids [6–8] and liquid-crystals. [9, 10] The intrinsic conflict of two-dimensional ordering and substrate curvature creates unique stress patterns. [11, 12] Especially, resolving the accumulated stress in regular particle arrays leads to rich physics associated with the elastic [11, 13] and plastic [12, 14–16] response of the system, which also underlies a host of problems in materials geometry. Examples include the curvature driven patterned deformations [11, 13, 17] and the exceedingly rich topological defect structures. [7, 18–20] While much has been learned about the elastic patterns and defect motifs in curved 2D crystals, [1, 2, 21] the microscopic process of the transition from the elastic deformation to the yield of the crystalline order and its connection with stress has not yet been fully explored.

The goal of this work is to elucidate these fundamental questions regarding the adaptivity of crystalline order on curved space. [14, 15] The spherical crystalline cap provides a suitable model to address these questions. [11, 14, 15] The crystalline cap is composed of a regular array of point particles that interact by the Lennard-Jones (L-J) potential. [22] In this work, by applying the fixed boundary condition, the stretching of the cap could be precisely controlled by shrinking the sphere. By the combination of geometric analysis and elasticity theory, we analytically analyze the inhomogeneous packings of the particles in mechanical equilibrium, reveal the quasi-conformal ordering underlying the inhomogeneous lattice, and discover the partial, but uniform screening of the substrate curvature by the inhomogeneity-induced curvature. This scenario is fundamentally different from the conventional screening mechanism based on topological defects. [23, 24] The highly stressed cap ultimately experiences plastic deformation. The featured morphol-

ogy of the fracture and the associated energetics are discussed. We also demonstrate the strategy of exploiting the stress-concentration effect of vacancies [25, 26] to engineer stress and fractures. This work demonstrates the rich physics in the deformations of crystalline caps, and may have implications in the engineering of extensive crystalline materials.

II. MODEL AND METHOD

In our model, the L-J potential allows us to conveniently explore both the elastic and plastic regimes; the formally simple L-J potential has also been extensively used to model various chemical and physical bonds. [27] $V_{L-J}(r) = \varepsilon_0[(r_m/r)^{12} - 2(r_m/r)^6]$, where r is the Euclidean distance between two particles, r_m is the equilibrium distance, and $-\varepsilon_0$ is the minimum potential energy. All of the particles are confined on the sphere of radius R by geometric constraint without resorting to any external potential. The particles on the boundary annulus of the cap are anchored, which constitutes the fixed boundary condition [see Fig. 1(a)]. The cap is stress free in the limit of infinitely large R . The degree of the stretching is characterized by $\gamma = (\omega_0 - \rho_0)/\rho_0$, where ρ_0 is the radius of the circular boundary and ω_0 is the geodesic radius of the spherical cap. $\omega_0 = R \arcsin(\rho_0/R) \approx \rho_0 + K_s \rho_0^3/6$, where K_s is the Gaussian curvature of the spherical substrate of radius R . [28] $\omega_0 = \rho_0$ as $R \rightarrow \infty$. In simulations, the radius of the sphere is gradually reduced. For each given R , the system is fully relaxed to the lowest energy state by the movement of the particles on the surface of the sphere according to the high-precision steepest descent method. [29–31] In this work, the units of length and energy are r_m and ε_0 .

III. RESULTS AND DISCUSSION

We first analytically analyze the elastic deformation of the crystalline cap by the continuum elasticity theory. The packing of the L-J particles in mechanical equi-

* zyao@sjtu.edu.cn

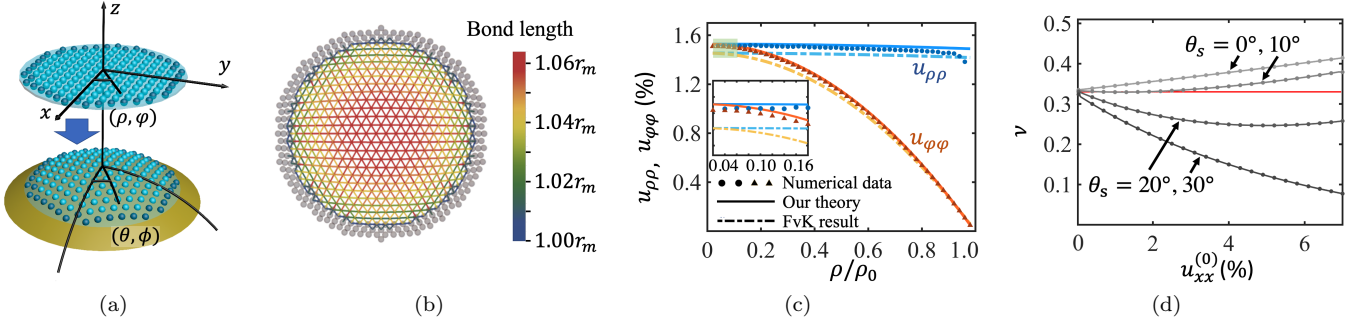


FIG. 1. Elastic deformation of the crystalline cap confined on the sphere. (a) A schematic plot of the crystalline cap model. The darker dots represent the anchored boundary particles. Polar coordinates (ρ, φ) and spherical coordinates (θ, ϕ) are established over the undeformed planar disk and the deformed cap, respectively. Note that $\varphi = \phi$ due to the rotational symmetry in the deformation. (b) The top view of an inhomogeneously stretched L-J crystalline cap in mechanical equilibrium. $\gamma = 5.95\%$. $\rho_0 = 10r_m$. $R = 18.1r_m$. (c) The strain field in the stretched cap. $\gamma = 1.5\%$. $\rho_0 = 50r_m$. $R = 170.1r_m$. $\nu_{\text{eff}} = 0.31$. (d) Dependence of the Poisson's ratio on the preset strain $u_{xx}^{(0)}$ of a planar triangular L-J lattice. θ_s is the angle of the direction of stretching and the principal axis of the lattice (the x-axis). The red line at $\nu = 1/3$ indicates the reference value of the Poisson's ratio for the isotropic elastic medium composed of linear springs in triangular lattice.

librium is determined by the force balance equations in terms of the stress tensor $\boldsymbol{\sigma}$. [26] In spherical coordinates (θ, ϕ) , the in-plane force balance equation of $\nabla \cdot \boldsymbol{\sigma} = 0$ becomes

$$\partial_\theta \sigma_{\theta\theta} + \partial_\phi \left(\frac{\sigma_{\theta\phi}}{\sin\theta} \right) + \cot\theta (\sigma_{\theta\theta} - \sigma_{\phi\phi}) = 0, \quad (1)$$

$$\partial_\theta \sigma_{\theta\phi} + \frac{1}{\sin\theta} \partial_\phi \sigma_{\phi\phi} + 2 \cot\theta \sigma_{\theta\phi} = 0. \quad (2)$$

To deal with the boundary condition, we express the force balance equations in terms of the displacement u_ρ over the undeformed planar disk, where the polar coordinates (ρ, φ) are established [see Fig. 1(a)]. The detailed derivation is presented in Supplemental Material. [31, 32] By applying the boundary conditions of $u_\rho(0) = u_\rho(\rho_0) = 0$ and making use of the rotational symmetry of the system, we obtain the analytical expressions for the strain field up to $(\rho_0/R)^4$:

$$u_{\rho\rho} = \frac{3-\nu}{16} \left(\frac{\rho_0}{R} \right)^2 + \left[\frac{7(3-\nu)^2}{512} \left(\frac{\rho_0}{R} \right)^4 \right] + \left\{ \frac{3\nu-1}{16} \left(\frac{\rho_0}{R} \right)^2 + \left[\frac{(3\nu-1)(3-\nu)}{64} \left(\frac{\rho_0}{R} \right)^4 \right] \right\} \frac{\rho^2}{\rho_0^2}, \quad (3)$$

$$u_{\varphi\varphi} = \frac{3-\nu}{16} \left(\frac{\rho_0}{R} \right)^2 + \left[\frac{7(3-\nu)^2}{512} \left(\frac{\rho_0}{R} \right)^4 \right] + \left\{ \frac{\nu-3}{16} \left(\frac{\rho_0}{R} \right)^2 + \left[\frac{-(3-\nu)^2}{64} \left(\frac{\rho_0}{R} \right)^4 \right] \right\} \frac{\rho^2}{\rho_0^2}. \quad (4)$$

The shear components of the strain tensor are zero. In Eqs.(3) and (4), the terms in the square brackets are the

higher order correction terms in comparison with the conventional approximate solutions to the FvK equations. The FvK equations describe the out-of-plane deformation of plates. [26]. The axisymmetric form of the FvK equations is:[11, 33]

$$\frac{d}{d\rho} (\rho \sigma_{\rho\rho}) - \sigma_{\varphi\varphi} = 0, \quad (5)$$

$$B \Delta^2 \zeta - \sigma_{\rho\rho} \frac{d^2 \zeta}{d\rho^2} - \frac{\sigma_{\varphi\varphi}}{\rho} \frac{d\zeta}{d\rho} = F_N, \quad (6)$$

$\sigma_{\rho\rho}$ and $\sigma_{\varphi\varphi}$ are the in-plane stress tensors in polar coordinates on the undeformed plate. $\zeta(\rho)$ is the out-of-plane deformation. B is the bending modulus, F_N is the exerted normal force per unit area and Δ is the Laplacian operator. By expressing Eq. (5) in terms of u_ρ and applying the boundary conditions $u_\rho(0) = u_\rho(\rho_0) = 0$, we obtain the expressions for the strain field up to the order of $(\rho_0/R)^2$, as contained in Eqs. (3) and (4). [31]

Equations (3) and (4) show that the homogeneously curved substrate geometry creates an inhomogeneous strain field, which is fundamentally different from the case of a planar membrane under radial tension. Simulations confirm the inhomogeneous distribution of the L-J particles on the sphere, as shown in Fig. 1(b). Analysis of the bond length, which are constructed by the standard Delaunay triangulation procedure, [1] shows that the central region in the deformed lattice is subject to a stronger stretching. Furthermore, the ratio of the maximum to the minimum bond length in the equilibrium configuration increases with the value of γ , indicating that the degree of inhomogeneity is enhanced as the sphere shrinks.

In Eqs. (3) and (4), we notice that the strain field is completely determined by the Gaussian curvature $1/R^2$ of the substrate and the Poisson's ratio ν ; the Young's modulus does not enter the equation. It is known that

$\nu = 1/3$ for an isotropic elastic medium composed of linear springs in triangular lattice. [26, 34] However, since the residual strain could influence the value of ν , [35] could we still specify a uniform value to the Poisson's ratio for our system?

To address this question, we numerically study the dependence of the Poisson's ratio on the magnitude of the preset strain and the direction of stretching. The detailed information about the measurement of Poisson's ratio is presented in Supplemental Material. [31] From Fig. 1(d), we see that the nonmonotonous ν -curves converge to a common value that is very close to $1/3$ as $u_{xx}^{(0)}$ becomes vanishingly small. It suggests that the Poisson's ratio of a slightly stretched crystalline cap may be approximately specified by a uniform value. As such, the parameter ν appearing in Eqs.(3) and (4) shall be interpreted as an effective Poisson's ratio, [35] whose value is determined as $\nu_{\text{eff}} = 0.31$ by matching the analytical result and the simulation data for $\gamma = 1.5\%$. $\nu_{\text{eff}} = 0.31 \pm 0.01$ for $\gamma \in [1\%, 2\%]$.

We plot the theoretically obtained strain field in Fig. 1(c) by inserting the value of ν_{eff} into Eqs. (3) and (4). Comparison with the numerical results shows that the positive terms in the first square brackets in Eqs. (3) and (4) significantly reduce the gap between the analytical results based on the FvK equations and the simulation data.

Now, we resort to the geometric concepts of metric and curvature to analyze the deformed lattice of the L-J particles in mechanical equilibrium for fully understanding the inhomogeneity phenomenon. A key observation is that the distribution of the bond angle is sharply concentrated at $\pi/3$ for varying values of γ . [31] The deformation of the lattice is therefore approximately angle-preserved. [36, 37] In mathematics, strictly angle-preserved deformation is known as conformal transformation. Here, the quasi-conformal deformation of the

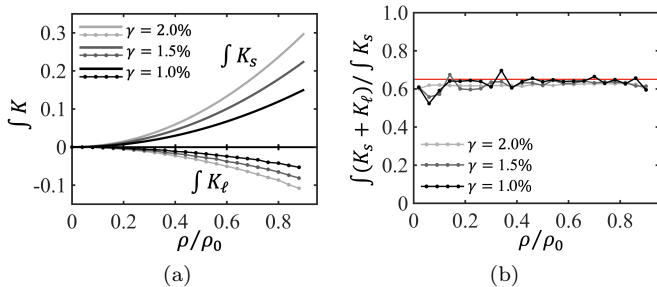


FIG. 2. Numerical simulations reveal the partial, but uniform screening of the substrate curvature K_s by the induced curvature K_ℓ underlying the inhomogeneous packings of the L-J particles. (a) Plot of the integrated K_s and K_ℓ at varying degrees of stretching. (b) Plot of the ratio of the excess integrated curvature and the integrated K_s . The stable curves indicate the uniform screening of the substrate curvature by K_ℓ . The red line indicates the theoretical value of 0.65. $\rho_0 = 50r_m$.

lattice allows us to approximately construct the metric of the following form on the undeformed planar disk:

$$ds^2 = \Lambda(\rho)^2(d\rho^2 + \rho^2 d\varphi^2), \quad (7)$$

where $\Lambda = dl/dl'$. dl and dl' are the length of the line element at ρ before and after the deformation, respectively. Equation 7 represents a purely geometric approach to understanding the deformation of the lattice.

According to the Gauss's Theorema Egregium, the Gaussian curvature is solely determined by the metric. [38] As determined by Eq. (7), the Gaussian curvature K_ℓ associated with the intrinsic inhomogeneity of the lattice (regardless of its shape in three-dimensional Euclidean space) is: [39, 40]

$$K_\ell = -\frac{1}{2}\Delta \ln \frac{\eta(\rho)}{\eta_0}, \quad (8)$$

where the ratio of the densities $\eta(\rho)/\eta_0 = \Lambda(\rho)^{-2}$. η_0 is the density of the undeformed lattice. Δ is the Laplacian operator. The subscript in K_ℓ is to indicate that this curvature is associated with the lattice; the Gaussian curvature of the spherical substrate is denoted as K_s . From the geometric perspective, by stretching the lattice, the spherical substrate essentially induces a Gaussian curvature in the resulting inhomogeneous lattice. Could the induced Gaussian curvature K_ℓ , as governed by the mechanical law, fully screen the curvature of the substrate geometry? In other words, is $K_\ell = -K_s$?

To address this question, we further analyze the simulation data to address inquiry into the nature of the induced curvature K_ℓ . The plot of the integrated curvatures is presented in Fig. 2(a). First of all, we see that the sign of K_ℓ is negative over the entire lattice at varying degrees of stretching. But the magnitude of the integrated K_ℓ is always smaller than the integrated K_s . In other words, the curvature of the spherical substrate could not be fully screened by the induced curvature. From Fig. 2(b), we see that the ratio of the excess integrated curvature and the integrated K_s is rather stable. It implies that the inhomogeneity created in the deformed lattice is to uniformize the screening of the substrate curvature, although this screening is not complete.

To explore the physical origin of the partial, but uniform screening phenomenon, we first establish the relation between K_ℓ and the strain tensor under the small deformation approximation: [31]

$$K_\ell = \frac{1}{2} \left[\frac{1}{\rho} \frac{d}{d\rho} (u_{\rho\rho} + u_{\varphi\varphi}) + \frac{d^2}{d\rho^2} (u_{\rho\rho} + u_{\varphi\varphi}) \right], \quad (9)$$

Note that Eq. (9) could be used to analyze the intrinsic curvature structure in a series of problems related to the wrinkling of circular sheets under tension or in differential growth. [41, 42] Inserting Eqs. (3) and (4) into Eq. (9), we have

$$\frac{K_s + K_\ell}{K_s} = \frac{1 + \nu}{2} + O\left(\frac{\rho_0^2}{R^2}\right). \quad (10)$$

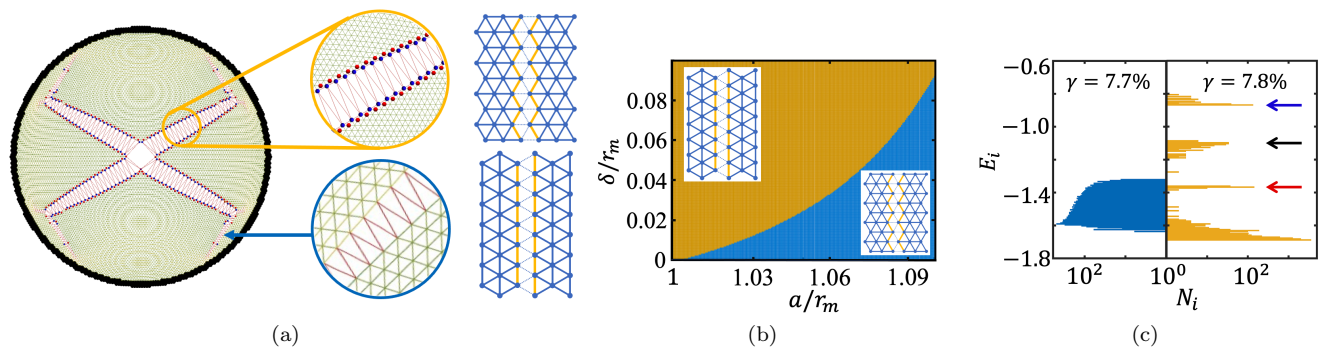


FIG. 3. The yield of the crystalline cap with the shrinking of the sphere. (a) A typical fracture pattern featured with a 90° turn at the tip. The insets show the zigzag and flat fractures. The red and blue dots represent five- and seven-fold disclinations. $\gamma = 7.8\%$. $\rho_0 = 50r_m$. (b) The phase diagram for the emergence of zigzag and flat fractures in the isotropically stretched planar L-J lattice of lattice spacing a . δ is the relative displacement of the crystals separated by the yellow boundaries. (c) The redistribution of the energy of individual particles caused by the rupture event. The single-peak profile prior to rupture ($\gamma = 7.7\%$) splits into multiple energy bands at $\gamma = 7.8\%$. N_i is the number of particles whose energy is in the range of $E_i \pm \delta E/2$. $\delta E = 0.015$. The elevated energy bands indicated by the blue and red arrows correspond to the particles of the same color along the zigzag fractures; see the upper circle in (a). And the energy band indicated by the black arrow corresponds to the particles along the flat fracture; see the lower circle in (a). $\rho_0 = 50r_m$.

Equation (10) clearly shows that $K_\ell \neq -K_s$ in general. K_ℓ is determined by both the curvature of the substrate and microscopic interaction; the later effect is reflected in the quantity of the Poisson's ratio according to Eq. (10). Here, it is of interest to note that the amount of excess curvature is completely determined by the Poisson's ratio, and it is independent of other elastic moduli of the material. For our elastic cap system, where $\nu_{\text{eff}} = 0.31$, the relative excess curvature is about 0.65 by Eq. (10). This result agrees well with the simulation data in Fig. 2.

Here, we shall emphasize that the screening mechanism by creating inhomogeneity with quasi-conformal ordering occurs in the elastic regime, and it is fundamentally different from the conventional screening scenario of plastic deformation based on topological defects. [23, 24] In the plastic deformation of geometrically frustrated 2D crystals on curved space, topological defects tend to proliferate to screen the Gaussian curvature of the substrate surface to minimize the elastic free energy. [23, 24] In our system, the proliferation of topological defects is suppressed under the fixed boundary condition. Our previous study on the frustration of L-J crystal clusters on the sphere shows that, under the stress-free boundary condition, the appearance of interior dislocations accompanies the formation of step structures along the cluster contour. [15] The fixed boundary condition forbids the relative displacement of the boundary particles, and thus suppresses the proliferation of interior topological defects. As such, the crystalline cap system deactivates the screening mechanism based on topological defects, and adopts the fashion of creating inhomogeneity to fit the curved substrate.

We proceed to explore the plastic deformation regime, where the highly stretched crystalline cap ultimately yields under the accumulated stress. Simulations show

that the cap is fractured as the value of γ exceeds 7.8%, regardless of the relative position of the entire lattice with respect to the center of the cap. The global rupture of the cap is triggered by slightly increasing γ at the rate of $\delta\gamma$; $\delta\gamma$ is at the order of 10^{-6} . A typical fracture pattern is shown in Fig. 3(a); fracture patterns with three branches are also observed. [31] It is uniformly observed that the fracture takes a 90° turn near the boundary. The radial and azimuthal fractures occur simultaneously. In this turning, the microscopic morphology of the fracture transforms from the zigzag to the flat type, as illustrated in Fig. 3(a).

To understand the formation of the featured rupture mode in Fig.3(a), we first analyze the strain field in the central region. This region is isotropically stretched, and it is subject to maximum stretching according to the solved strain field. In an isotropically stretched two-dimensional crystal, which type of fracture will cost less energy? To address this question, we perform numerical experiment with a planar L-J lattice under isotropic stretching whose lattice spacing is a . By comparing the energies of creating zigzag and flat fractures of separation δ , we obtain the phase diagram in Fig.3(b). It turns out that the zigzag fracture is relatively energetically favored. This explains the observed zigzag fracture in the central region of the cap.

The turning of the fracture is driven by the highly anisotropic strain field near the boundary of the cap, as shown in the $u_{\rho\rho}$ and $u_{\varphi\varphi}$ curves in Fig.1(c). Under the much larger radial strain $u_{\rho\rho}$, the lattice tends to break along the azimuthal direction. To conclude, the microscopic crystalline structure determines the morphology of the central fracture pattern, and the anisotropy of the strain field is responsible for the turning of the fracture near the boundary. The remarkable coexistence of the

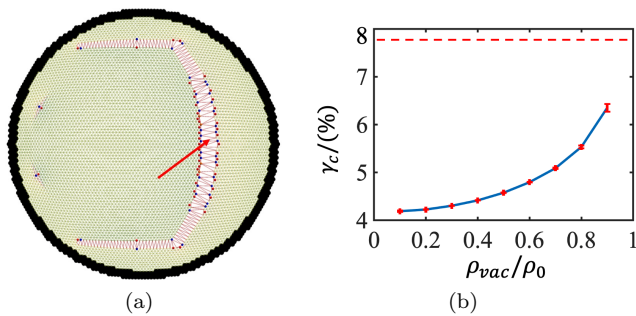


FIG. 4. Controlling the fracture pattern and plastic deformation by exploiting the stress-concentration effect of the vacancy. (a) The presence of the vacancy, whose location is indicated by the arrow, leads to a fracture pattern that is distinct from the case of the vacancy-free cap in Fig. 3a. The red and blue dots represent five- and seven-fold disclinations. $\gamma = 4.6\%$. $R = 101.4r_m$. (b) Plot of the critical value for γ versus the location of the vacancy. The dashed red line indicates the value of $\gamma_c = 7.8\%$ for the case of the vacancy-free cap. $\rho_0 = 50r_m$. The error bars are obtained by statistical analysis of the cases where the relative position of the entire lattice with respect to the center of the cap is randomly specified.

radial and azimuthal fractures, which is absent in planar systems, is essentially originated from the confluence of elasticity, curvature and the microscopic crystalline structure. Note that curvature-driven fracture phenomena are also reported in the deformation of nanoparticle monolayers [43] and the 2D crystallization on the sphere. [44]

Now, we discuss the energetics in the fracture of the crystalline cap. Simulations show that the rupture event fundamentally changes the energy landscape. The redistribution of the energy among individual particles is summarized in Fig. 3(c). We see that the original single-peak profile splits into multiple energy bands. Some particles jump to a few higher energy bands, but the energy of most particles is lowered. The total energy of the system is significantly reduced by 8%. We also notice that the width of the original energy profile shrinks in this process, indicating a reduced discrepancy in the energy of the particles occupying the same energy band.

The stress-steered rupture of the cap inspires us to explore the notion of actively controlling the fracture by engineering the stress over the surface. Specifically, we propose the strategy of introducing microscopic vacancies and exploiting the stress-concentration effect to redistribute the stress and guide the formation of the frac-

ture. [25, 45]

A vacancy is created by removing a single particle in the crystalline cap. In the presence of the vacancy, whose location is indicated by the arrow in Fig. 4(a), the resulting fracture pattern is completely different from the case in Fig.3(a). The formation of the new pattern is attributed to the vacancy-driven amplified discrepancy of the radial and azimuthal strains surrounding the vacancy. The dominant radial strain ultimately leads to the azimuthal fracture passing through the vacancy. [25] Instabilities caused by the stress-focusing effect of vacancies are also found in particulate elastic systems. [45] Simulations further show that introducing a vacancy, especially near the center of the cap, could significantly reduce the strength of the cap, as shown in Fig.4(b). The dashed line in Fig.4(b) indicates the value of γ_c for the case of vacancy-free cap. It is remarkable that the microscopic operation of removing a single particle leads to macroscopic effects in both aspects of fracture pattern and material strength. More examples of fracture patterns as controlled by the number and locations of vacancies are provided in Supplemental Material. [31]

IV. CONCLUSIONS

In summary, we have used the crystalline cap model to reveal the generic behaviors in the adaptivity of the two-dimensional crystalline systems on curved space in both elastic and plastic regimes. In the elastic regime, the geometric concepts of metric and curvature provide a vigorous formalism for understanding the observed inhomogeneous organization of the particles in the quasi-conformal lattice. In the plastic regime, we observe the microscopic yield of highly stressed caps, rationalize the emergence of the fracture patterns, and demonstrate the strategy of exploiting the stress-concentration effect of vacancies to actively control the fractures. This work shows the essential role of geometry to foster insights into the deep connection between inhomogeneity, stress and curvature.

ACKNOWLEDGEMENTS

This work was supported by the National Natural Science Foundation of China (Grants No. BC4190050). The authors acknowledge the support from the Student Innovation Center at Shanghai Jiao Tong University.

[1] D. R. Nelson, *Defects and Geometry in Condensed Matter Physics* (Cambridge University Press, Cambridge, 2002).
 [2] M. J. Bowick and L. Giomi, *Adv. Phys.* **58**, 449 (2009).
 [3] D. L. D. Caspar and A. Klug, *Cold Spring Harb. Symp. Quant. Biol.* **27**, 1 (1962).

[4] J. Lidmar, L. Mirny, and D. R. Nelson, *Phys. Rev. E* **68**, 051910 (2003).
 [5] R. Zandi, D. Reguera, R. F. Bruinsma, W. M. Gelbart, and J. Rudnick, *Proc. Natl. Acad. Sci. U.S.A.* **101**, 15556 (2004).

- [6] A. D. Dinsmore, M. F. Hsu, M. G. Nikolaides, M. Marquez, A. R. Bausch, and D. A. Weitz, *Science* **298**, 1006 (2002).
- [7] A. R. Bausch, M. J. Bowick, A. Cacciuto, A. D. Dinsmore, M. F. Hsu, D. R. Nelson, M. G. Nikolaides, A. Travesset, and D. A. Weitz, *Science* **299**, 1716 (2003).
- [8] D. Ershov, J. Sprakel, J. Appel, M. A. C. Stuart, and J. van der Gucht, *Proc. Natl. Acad. Sci. U.S.A.* **110**, 9220 (2013).
- [9] D. R. Nelson, *Nano Lett.* **2**, 1125 (2002).
- [10] A. Fernández-Nieves, V. Vitelli, A. S. Utada, D. R. Link, M. Márquez, D. R. Nelson, and D. A. Weitz, *Phys. Rev. Lett.* **99**, 157801 (2007).
- [11] G. M. Grason and B. Davidovitch, *Proc. Natl. Acad. Sci. U.S.A.* **110**, 12893 (2013).
- [12] A. Azadi and G. M. Grason, *Phys. Rev. Lett.* **112**, 225502 (2014).
- [13] G. Vernizzi, R. Sknepnek, and M. Olvera de la Cruz, *Proc. Natl. Acad. Sci. U.S.A.* **108**, 4292 (2011).
- [14] S. Li, R. Zandi, A. Travesset, and G. M. Grason, *Phys. Rev. Lett.* **123**, 145501 (2019).
- [15] Z. Yao, *Soft Matter* **13**, 5905 (2017).
- [16] N. P. Mitchell, V. Koning, V. Vitelli, and W. T. M. Irvine, *Nat. Mater.* **16**, 89 (2017).
- [17] Y. Klein, E. Efrati, and E. Sharon, *Science* **315**, 1116 (2007).
- [18] M. J. Bowick, A. Cacciuto, D. R. Nelson, and A. Travesset, *Phys. Rev. Lett.* **89**, 185502 (2002).
- [19] W. T. Irvine, V. Vitelli, and P. M. Chaikin, *Nature* **468**, 947 (2010).
- [20] H. Kusumaatmaja and D. J. Wales, *Phys. Rev. Lett.* **110**, 165502 (2013).
- [21] B. Audoly and Y. Pomeau, *Elasticity and Geometry* (Oxford University Press, Oxford, 2010).
- [22] J. E. Jones, *Proc. R. Soc. A* **106**, 463 (1924).
- [23] D. Nelson and L. Peliti, *J. Phys.* **48**, 1085 (1987).
- [24] M. J. Bowick, D. R. Nelson, and A. Travesset, *Phys. Rev. B* **62**, 8738 (2000).
- [25] S. P. Timoshenko and J. N. Goodier, *Theory of Elasticity* (McGraw-Hill Book Company, New York, 1970).
- [26] L. D. Landau and E. Lifshitz, *Theory of Elasticity* (Pergamon, London, 1959).
- [27] J. N. Israelachvili, *Intermolecular and Surface Forces*, 3rd ed. (Academic Press, 2011).
- [28] M. P. do Carmo, *Differential geometry of curves and surfaces*. (Prentice Hall, 1976) pp. I–VIII, 1–503.
- [29] J. A. Snyman and D. N. Wilke, *Practical Mathematical Optimization* (Springer, New York, 2005).
- [30] Z. Yao and M. Olvera de la Cruz, *Phys. Rev. Lett.* **116**, 148101 (2016).
- [31] See Supplemental Material for technical details about the numerical simulation, the analytical elastic and geometric analysis, and more information about the fracture patterns.
- [32] T. Belytschko, W. K. Liu, B. Moran, and K. Elkhodary, *Nonlinear Finite Elements for Continua and Structures* (John Wiley & Sons, New York, 2013).
- [33] H. King, R. D. Schroll, B. Davidovitch, and N. Menon, *Proc. Natl. Acad. Sci. U.S.A.* **109**, 9716 (2012).
- [34] H. S. Seung and D. R. Nelson, *Phys. Rev. A* **38**, 1005 (1988).
- [35] G. N. Greaves, A. Greer, R. S. Lakes, and T. Rouxel, *Nat. Mater.* **10**, 823 (2011).
- [36] F. Rothen, P. Pieranski, N. Rivier, and A. Joyet, *Eur. J. Phys.* **14**, 227 (1993).
- [37] P. Pieranski, in *Phase Transitions in Soft Condensed Matter*, edited by R. Tormod and S. David (Springer, New York, 1989) pp. 45–48.
- [38] D. Struik, *Lectures on Classical Differential Geometry*, 2nd ed. (Dover Publications, New York, 1988).
- [39] A. Mughal and M. A. Moore, *Phys. Rev. E* **76**, 011606 (2007).
- [40] V. Soni, L. R. Gomez, and W. T. Irvine, *Phys. Rev. X* **8**, 11039 (2018).
- [41] E. Cerda and L. Mahadevan, *Phys. Rev. Lett.* **90**, 074302 (2003).
- [42] E. Sharon, B. Roman, and H. L. Swinney, *Phys. Rev. E* **75**, 046211 (2007).
- [43] N. P. Mitchell, R. L. Carey, J. Hannah, Y. Wang, M. Cortes Ruiz, S. P. McBride, X.-M. Lin, and H. M. Jaeger, *Soft Matter* **14**, 9107 (2018).
- [44] L. Ortellado, D. A. Vega, and L. R. Gómez, *Phys. Rev. E* **105**, 014801 (2022).
- [45] Z. Yao, *Soft Matter* **16**, 5633 (2020).